Remote Sensing of Environment 163 (2015) 140–152

Contents lists available at ScienceDirect

Remote Sensing of Environment

journal homepage: www.elsevier.com/locate/rse

Global burned area mapping from ENVISAT-MERIS and MODIS active fire data

Itziar Alonso-Canas *, Emilio Chuvieco

Environmental Remote Sensing Research Group, Dep. of Geology, Geography and the Environment, University of Alcalá, c/Colegios 2, 28801 Alcalá de Henares, Spain

ARTICLE INFO

Article history:
Received 28 July 2014
Received in revised form 13 March 2015
Accepted 14 March 2015
Available online 4 April 2015

Keywords:
Fire
Biomass burning
MERIS
MODIS HS
Burned area

ABSTRACT

We present the development of a global burned area (BA) algorithm based on MERIS imagery along with the assessment of the global BA results for three years (2006–2008). This work was developed within the Fire Disturbance project under the European Space Agency Climate Change Initiative programme, which aimed to generate long-term BA information for climate models. Our algorithm combined temporal series of MERIS reflectances with thermal information from MODIS HS (hotspot) product. The algorithm included two-steps. Firstly, cumulative distribution functions were computed to discriminate the most clearly burned pixels using regionally-oriented near infrared reflectance thresholds. Secondly, a contextual criterion improved the spatial detection of the burned patches from the seed pixels. BA estimates for the three target years range from 3.6 to 3.8 million km^2. Results were validated from a statistically designed sample of fire perimeters generated from Landsat multi-temporal imagery. Intercomparison with existing BA products was also carried out. Results from global validation datasets provided an average overall accuracy higher than 0.95. The accuracy of the BA category was lower than the accuracy of the unburned one. Within the former, average omission and commission errors were lower for areas where the proportion of burned area was higher (for pixel-based error matrices, commission error (CE) was 0.52 and omission error (OE) was 0.51), than for those areas with very low BA proportion (CE = 0.60 and OE = 0.74). In terms of total BA estimation, errors were generally well balanced, with a tendency towards underestimation (34%). Relevant impact of temporal reporting accuracy was found for these validation datasets. Intercomparison with other existing BA datasets pointed out similar spatial and temporal trends, with high correlation with GFED v4 BA estimations for the three years ($r^2 > 0.974$).

1. Introduction

Fire is a key component of the carbon cycle, related to greenhouse gases and aerosol emissions to the atmosphere (Andreae & Merlet, 2001; van der Werf et al., 2010). Biomass burning has a critical relevance for global vegetation dynamics (Kloster, Mahowald, Randerson, & Lawrence, 2012; Thonicke et al., 2010), increasingly affecting human lives and property (Bowman et al., 2009).

Even though the current understanding of climate–fire interactions is limited, there is also increasing evidence on their mutual influence (Kloster et al., 2012; Krawchuk, Moritz, Parisien, Van Dorn, & Hayhoe, 2009; Mouillot & Field, 2005; Pechony & Shindell, 2010; Running, 2006). Expected temperature and rainfall changes are likely to increase wildfire frequency in some regions, while others may experience decrease in fire activity as a result of decreased biomass production (Daniau A.L., Bartlein P.J., Harrison S.P., Prentice I.C., Brewer S., Friedlingstein P., et al., 2012; Krawchuk et al., 2009).

The growing interaction between fire and climate highlights the relevance of accessing global burned area (BA) information, particularly for climate and dynamic vegetation models (Mouillot et al., 2014). The extended use of these models emphasises the need to have long-term and consistent time series of BA information, with proper error and uncertainty characterisation. This is the main goal of the Fire Disturbance (fire_cci) project (http://www.esa-fire-cci.org/ last accessed November 26, 2014). Fire is one of the Essential Climate Variables (ECV) within the European Space Agency Climate Change Initiative (ESA-CCI). The ESA-CCI is part of the European contribution to the Global Climate Observing System (GCOS) programme. Currently, the ESA CCI programme includes 13 ECVs that involve atmospheric (ozone, greenhouse gases, aerosols and clouds), oceanic (ocean colour, sea ice, ocean height and temperature), and terrestrial products (fire, glaciers, ice sheets, soil moisture and land cover) (Hollmann et al., 2013). The objective of the fire_cci project was to improve global mapping of BA and the use of this information in global vegetation and atmospheric models. This project aimed at developing burned area (BA) information from European medium resolution sensors: (A)ATSR (Advanced Along Track Scanning Radiometer) on board ERS (European Remote Sensing) and ENVISAT (Environmental Satellite), VEGETATION (VGT) on board the SPOT (Satellite Pour

* Corresponding author.
E-mail addresses: itziar.alonsoc@uah.es (I. Alonso-Canas), emilio.chuvieco@uah.es (E. Chuvieco).

http://dx.doi.org/10.1016/j.rse.2015.03.011
0034-4257/

l'Observation de la Terre) and MERIS (MEdium Resolution Imaging Spectrometer) on board ENVISAT. Following user recommendations, BA information should be offered at pixel level (monthly products at full resolution: 1000 m for VGT and ATSR and 300 m for MERIS) and grid level (fortnightly products at 0.5° cell resolution) retaining in both cases the date of detection. Both products included a set of auxiliary variables to facilitate their use by the climate modelling community (http://www.esa-fire-cci.org/webfm_send/771 last accessed November 26, 2014).

Monitoring areas affected by biomass burning has been performed over the last decades using a wide variety of sensors, from very high-spatial resolution such as Ikonos for fine scales (Kachmar & Sanchez-Azofeifa, 2006), to medium resolution sensors such as Landsat-TM/ETM + or SPOT-HRV for regional coverages (Bastarrika, Chuvieco, & Martin, 2011b; Pu & Gong, 2004) and to coarse spatial resolution sensors for continental to global studies (Chang & Song, 2009; Chuvieco et al., 2008; Giglio et al., 2010; Roy, Boschetti, & Justice, 2008; Tansey et al., 2008). The latter are the most relevant within the context of climate modelling and they are commonly offered in coarser resolution grids (0.25 to 0.5° cell).

The first attempts to globally map burned areas were based on NOAA (National Oceanic and Atmospheric Administration)-AVHRR (Advanced Very High Resolution Radiometer) data, mostly using multi-temporal changes of vegetation indices (Kasischke et al., 1993), although hybrid algorithms based on thermal and optical channels were also developed (Fraser, Li, & Cihlar, 2000; Roy, Giglio, Kendall, & Justice, 1999). Extensive regions were mapped from AVHRR HRPT (High Resolution Picture Transmission) (1.1 km at nadir) temporal series, especially in the boreal forest of Russia (Sukhinin et al., 2004) and Canada (Fraser et al., 2000). A few studies were also undertaken to map global BA using degraded spatial resolution AVHRR products, such as the 8 km PAL (Pathfinder Land) or LTDR (Long Term Data Record) series (Carmona-Moreno et al., 2005; Riaño, Ruiz, Isidoro, Ustin, & Riaño, 2007).

More recently, other sensors with greater sensitivity for mapping burned patches have been used to create global inventories of BA (Table 1). The GBA2000 was produced from VGT data of the year 2000, using a set of regional algorithms based on multi-temporal changes in daily reflectances or spectral indices (Tansey et al., 2004). This product was later extended to the 2000–2007 series and named L3JRC, still based on VGT data (Tansey et al., 2008). The ESA promoted another global BA product, named GLOBSCAR (Simon, Plummer, Fierens, Hoelzemann, & Arino, 2004), based on day time ATSR-2 images. Later, the approaches of these two European projects were combined within the Globcarbon project, which produced a 1998–2007 BA product based on both ATSR and VGT data (Plummer et al., 2007). More recently, the Copernicus land product services has released the Geoland BA variable, based on SPOT-VGT. In addition to European products, MODIS (MOderate Resolution Imaging Spectroradiometer) data on board the NASA (National Aeronautics and Space Administration) Terra and Aqua satellites have shown great potential for global mapping of BA. Currently, two MODIS global BA products are available. The standard one, named MCD45A1, is based on temporal differences of observed versus predicted reflectance using the inversion of a bidirectional reflectance model (Roy, Jin, Lewis, & Justice, 2005). The second one, the MCD64, is part of the Collection 5.1 Direct Broadcast products, and it is based on a hybrid algorithm combining active fire detections and multi-temporal changes in spectral indices (Giglio, Loboda, Roy, Quayle, & Justice, 2009). This product is the basis for the BA estimation included in the GFED (Global Fire Emissions Database) (Giglio et al., 2010), widely used by climate and carbon modellers.

All these global products have strengths and weaknesses and have been used in a wide range of modelling efforts (Mouillot et al., 2014). A proper validation and inter-comparison of all these products are still to be done, although regional comparisons have already been published (Boschetti, Eva, Brivio, & Gregoire, 2004; Roy & Boschetti, 2009). Recent papers have shown the use of statistical design frameworks for validation of global BA products (Padilla, Stehman, & Chuvieco, 2014; Padilla et al., 2015).

The goal of this paper is to present a global BA algorithm specifically tailored for the ENVISAT MERIS sensor in the context of the fire_cci project. MERIS was mainly designed for ocean colour applications, and provides high spectral resolution (Table 2) in the range of the blue to the near infrared regions (Gower & Borstad, 2004). The spatial resolution is 300 m in the full resolution mode (FRS) and 1200 m in the Reduced Resolution (RR) mode. The total field of view of MERIS is 68.5° around nadir, covering a swath width of 1150 km, and yielding to a 3 day revisit time for equatorial regions. The application of MERIS data to fire applications is scarce: identification of smoke plumes (Huang & Siegert, 2004) and discrimination of burn severity (Chuvieco, De Santis, Riaño, & Halligan, 2007; Roldan-Zamarron, Merino-De-Miguel, Gonzalez-Alonso, Garcia-Gigorro, & Cuevas, 2006). Mapping BA with MERIS was performed only at regional level (Oliva, Martin, & Chuvieco, 2011) using different vegetation indices, while González-Alonso et al. (2009) combined fire hotspots from MODIS and near infrared (NIR) reflectance values from MODIS and MERIS imagery.

MERIS presents some challenges for mapping burned areas. Spectral and temporal resolutions are not ideal for BA discrimination, as the sensor does not include short-wave infrared bands and global coverage of the Earth is obtained every three days. However, the potential of MERIS for improving current information of BA relies on its greater spatial resolution in the FRS mode (used throughout this paper), thus

Table 1
Summary of existing BA products.

	Sensor	Time series	Spatial res	Type of algorithm/detection	Reference
MCD 45	MODIS Aqua Terra	2001–present	500 m	Bi-directional reflectance model-based change detection approach	Roy et al. (2005)
MCD 64	MODIS Aqua Terra	2001–present	500 m	HS and multi temporal spectral indices changes	Giglio et al. (2009)
GBA 2000	SPOT VGT	11/1999–12/2000	1 km	Multi temporal changes in daily reflectances or spectral indices (IFI and UTL algorithms)	Ershov and Novik (2001) Silva et al. (2003) Grégoire, Tansey, and Silva (2003)
GBS	NOAA AVHRR	1982–1999	8 km	Multi temporal change detection	Carmona-Moreno et al. (2005)
GLOB SCAR	ERS2 ATSR2	2000	1 km	K1: contextual algorithm based on geometrical characteristics of burned pixels in the near-infrared (NIR, 0.87 μm)/thermal infrared (TIR, 11 μm). E1: series of fixed thresholds applied to the data from four spectral channels.	Piccolini and Arino (2000) Eva and Lambin (1998)
GLOB CARBON	ERS2 ATSR2 SPOT VGT ENVISAT AATSR	1998–2007	1 km	Based on two GBA2000 algorithms: IFI and UTL and two GLOBSCAR algorithms: K1 and E1.	
L3JRC	SPOT VGT	2000–2007	1 km	Temporal index, based on GBA2000 experience.	Tansey et al. (2008)
GEO LAND2	SPOT VGT	1999–present	1 km	Temporal index and thresholds	(http://www.geoland2.eu/ last accessed November 26, 2014)

Table 2
MERIS bands characteristics.

Band	Band centre (nm)	Bandwidth (nm)
1	412.5	10
2	442.5	10
3	490	10
4	510	10
5	560	10
6	620	10
7	665	10
8	681.25	7.5
9	705	10
10	753.75	7.5
11	760	2.5
12	775	15
13	865	20
14	890	10
15	900	10

potentially providing better detection of small burn patches than coarser resolution sensors. Furthermore, this sensor has a follow up version on the OLCI (Ocean and Land Colour Instrument) sensor, and will be complemented with the SLSTR (Sea and Land Surface Temperature Radiometer), both payloads on board Sentinel 3, scheduled for launch in 2015 within the EC Copernicus programme.

2. Methods

2.1. Framework

The design of a global BA algorithm requires considering the great diversity of biomass burning conditions worldwide. The most extended approaches for mapping BA can be classified in two groups: those that use the thermal contrast of active fires (commonly named hot spots, HSs) from the surrounding background (Giglio et al., 2006b), and those based on reflectance changes caused by burning effects (changing of leaf and soil colour, leaf losses, char background, etc.) (Bastarrika, Chuvieco, & Martin, 2011a; Roy et al., 2005). The former approach is more reliable because thermal radiance (and consequently the signal amplification) increases exponentially with temperature, while fire-related reflectance changes are more subtle. However, thermal signal lasts very shortly (minutes to hours) while the fires are active, whereas post-fire reflectance changes last much longer (days to years). In addition, BA mapping based on active fires only implies a sample of the total area burned (what is actually burning when the satellite observes the area), while reflectance changes are noticeable in the whole area affected by the fire (providing the impact of fire is severe enough).

Several authors have proposed hybrid algorithms to overcome the limitations of each approach. These algorithms commonly use HS information either to guide the characterisation of BA statistics or to confirm potential burned pixels. The use of thermal anomalies helps avoiding commission errors related to reflectance changes caused by non-fire events (such as crop harvest, seasonal flooding, or topographic shades), which are not associated to sharp increases of temperature. This hybrid approach was initially proposed for the AVHRR sensor (Fraser et al., 2000; Roy et al., 1999), with partial success, as the AVHRR thermal channel was not particularly suitable for detecting active fires. More recently, hybrid algorithms have been used to generate the MCD64 product (Giglio et al., 2009).

Considering the spectral and temporal limitations of MERIS, it was decided to develop the BA algorithm from a hybrid approach, using a combination of HS information derived from MODIS data (http://modis-fire.umd.edu/ last accessed January 27, 2015) and temporal trends of MERIS reflectance bands. In order to consider a proper balance between omission and commission errors, the algorithm included two different phases (Chuvieco, Englefield, Trishchenko, & Luo, 2008). First, a seed identification phase, which aimed to minimise commission by applying a series of criteria to determine those pixels that were most likely to be burned. Second, a contextual phase, which applied region growing analysis to improve the delimitation of burned patches. These two phase algorithms have been successfully used in previous BA studies (Bastarrika et al., 2011a; Chuvieco et al., 2008; Martín, Gómez, & Chuvieco, 2005). The algorithm was developed and tested in 10 different study sites, which were selected to take into account the diversity of burning conditions worldwide, including different biomes and fire regimes (Fig. 1).

2.2. Generation of corrected reflectances and spectral indices

Corrected MERIS reflectances were received from Brockmann Consult (http://www.brockmann-consult.de/ last accessed November 26, 2014). The pre-processing chain was based on the one developed for the Landcover CCI project, with modifications to obtain daily reflectances instead of weekly composites (as it was required by that project). Geometric correction was obtained through the AMORGOS software (Accurate MERIS Ortho Rectified Geo-location Operational Software, Bourg, 2011), improving MERIS FR geolocation (RMS < 70 m). Calibration and smile correction were also performed, as well as land water delineation, cloud screening and atmospheric correction (more details of these processes in http://www.esa-landcover-cci.org/?q=webfm_send/75 last accessed November 26, 2014). The surface directional reflectances were delivered as floats between 0 and 1. In addition to corrected reflectances, the images included a standard error associated to each band, as well as the Sun and satellite zenith and azimuth angles. A status layer was provided as well, with values 1 (clear land), 3 (snow/ice), or 0 (i.e. water, cloud, no observation). Output files were gridded into tiles of 10 × 10° (3600 × 3600 pixels at MERIS FRS spatial resolution). These tiles were the input files for all processes of our BA algorithm.

The NIR region was selected as main input for the algorithm, since this spectral band is highly sensitive to recent burns, as both green vegetation and dry vegetation have substantially higher reflectance than recent burns in the NIR (Chuvieco, Englefield, Trishchenko and Luo, 2008; Chuvieco, Martín, & Palacios, 2002; Koutsias & Karteris, 2000; Trigg & Flasse, 2001). In addition to the NIR band, we computed the Global Environmental Monitoring Index (GEMI) (Pinty & Verstraete, 1992), which was proven the best performing index to detect burned areas among the spectral indices based on the red-NIR space (Barbosa, Grégoire, & Pereira, 1999; Chuvieco, Englefield, Trishchenko and Luo, 2008; Chuvieco et al., 2002; Martín et al., 2005; Pereira, 1999). GEMI was computed as follows:

$$\mathrm{GEMI} = \eta(1-0.25\eta) - \frac{(\rho_R - 0.125)}{(1-\rho_R)}$$

$$\eta = \frac{2\left(\rho_{NIR}{}^2 - \rho_R{}^2\right) + 1.5\rho_{NIR} + 0.5\rho_R}{(\rho_R + \rho_{NIR} + 0.5)},$$

where ρ_{NIR} is the reflectance in the NIR (in our case MERIS band 10) and ρ_R is the reflectance in the red (MERIS Band 8). The selection of MERIS bands 8 (673.75 nm to 688.75 nm), and 10 (746.25 nm to 761.25 nm), was based on the results from Oliva et al. (2011), which showed that short NIR bands (bands 9 to 12) had better sensitivity than long NIR bands (bands 13 to 15) to discriminate BA (Table 2).

2.3. Temporal compositing

Temporal resolution of input data is an important aspect to consider when building a global BA algorithm, since the analysis of post-fire reflectance may be easily contaminated by clouds or weaken by quick vegetation recovery. Therefore, the number of observations is a limiting factor for detecting fires, particularly in Tropical regions, where

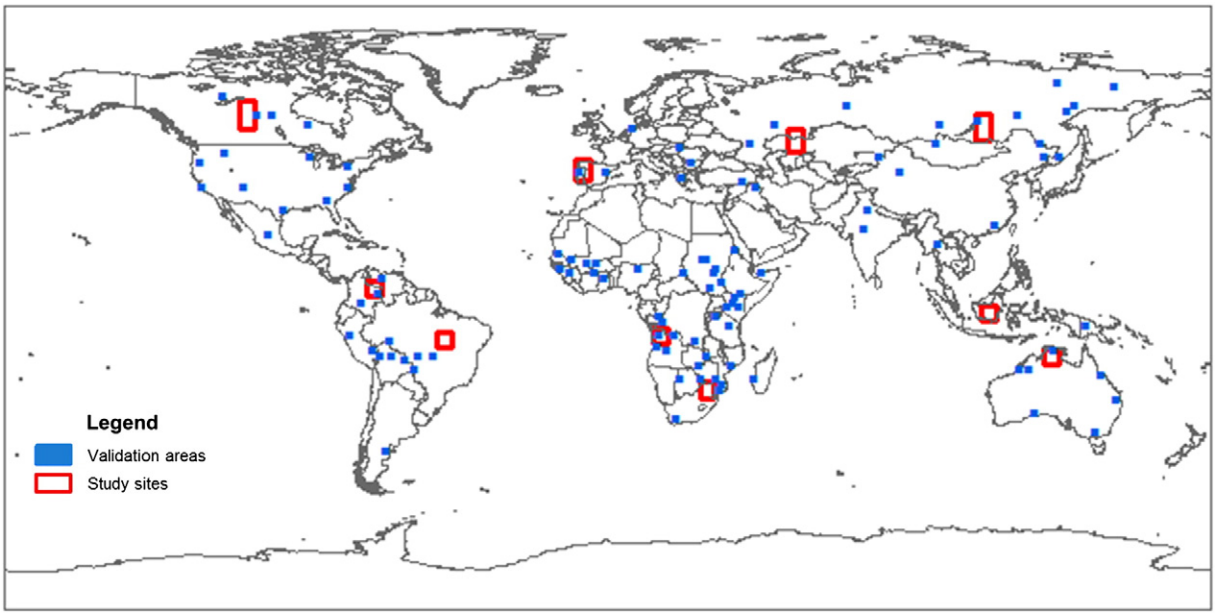

Fig. 1. Study and validation sites.

vegetation recovery is quite quick after fire. The MERIS sensor has a temporal resolution of 3 days at the Equator. In practice, taking into account cloud contamination and potential gaps in data reception, the temporal resolution becomes lower. Fig. 2 shows the maximum number of valid observations per month in 2008 for sample study sites of $10 \times 10°$ in different biomes.

Considering that some areas had little spatial continuity, we generated monthly composites of NIR to fill the potential gaps in day-to-day images, therefore improving the spatial coherence for BA detection. These composites were the basis for the two phases of the algorithm.

Different compositing techniques have been proposed in previous BA studies, most commonly maximising or minimising a certain input band to enhance the burned signal (Chuvieco, Ventura, Martín, & Gomez, 2005; Sousa, Pereira, & Silva, 2003). The criteria for generating the monthly NIR-GEMI composites were chosen as to emphasise the sensitivity of the outputs to the burned signal. Two criteria were used: maximise the proximity to fire dates and minimise the NIR signal. Both criteria aimed to select the most clearly burned pixel in the time series.

Since HS provide a very accurate estimation of burning dates (Boschetti, Roy, Justice, & Giglio, 2010), we first generated an auxiliary file selecting for each location the closest date to the closest HS. For doing so, a Thiessen matrix (Brassel & Reif, 1979) was created for each temporal composite labelling each pixel with the date of the closest HS. The Thiessen matrix was computed considering also those HS located within a buffer of 0.5° outside the edges of each tile. This option mitigated potential continuity problems between tiles, when for instance a fire occurred at the border of two tiles.

The second compositing criterion implied minimising the NIR reflectance values of the temporal series, as reflectance from a BA is expected to have a very low NIR value. However, since low NIR values can also be caused by other factors (cloud or topographic shadows, for instance), instead of selecting the minimum NIR of the period, we chose the first minimum after the date stored in the Thiessen HS file, as this would select a more immediate value to the post-fire burn reflectance. If no minima existed after that date, then the second minimum of the times series was chosen. Once the most suitable date for each pixel of the composite was obtained, two files were created, one with the NIR reflectance and the other one with the GEMI index for that particular date.

Composites were built for each month by selecting images from a bi-monthly time series (Fig. 3) to mitigate the impact of low MERIS temporal resolution, which is especially relevant for cloudy regions and for fires occurring at the end of the monthly period.

In addition to the monthly post-fire composites, an annual reference composite was created for the contextual phase of the algorithm. This annual composite maximised the GEMI value to account for the maximum seasonal greenness of each pixel. We assumed that the change between the annual maximum and the post-fire value (included in the GEMI monthly composite) should be the highest for burned pixels, thus emphasising post-fire spectral changes.

2.4. Seed selection phase

The first part of the seed selection focused on generating statistics of burned and unburned areas for each tile, based on the monthly composite NIR values and on the distribution of HS in the same month. Since burned conditions are very diverse worldwide, we aimed to obtain regional-

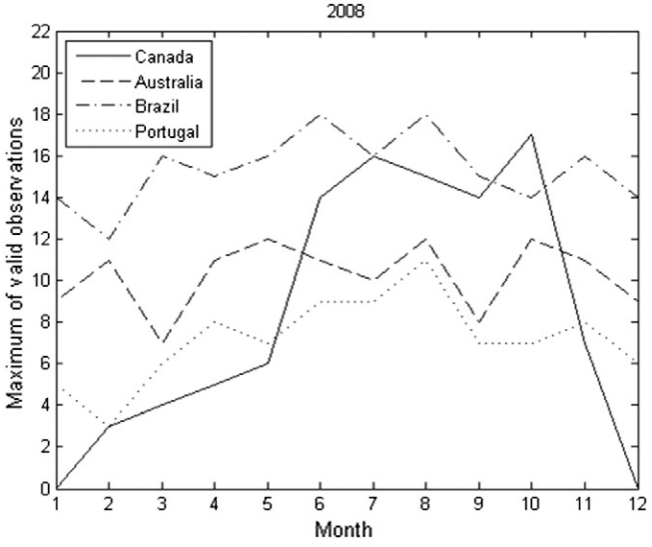

Fig. 2. Maximum number of MERIS valid observations per month in 2008. The areas selected are tiles of $10 \times 10°$ located in Canada (L03C07), Brazil (L09C20), Portugal (L05C17), and Australia (L10C31).

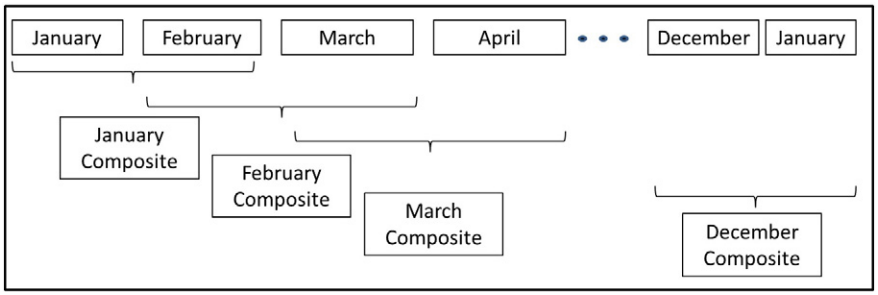

Fig. 3. Monthly composites generation based on MERIS information from two consecutive months.

oriented NIR thresholds, based on the 10 × 10° tiles, which should be adapted to different post-fire reflectance conditions. Cumulative distribution functions (CDFs) were created for each tile to establish regionally-oriented thresholds of NIR values, in order to emphasise discrimination between burned and unburned categories. Thresholds selected changed in each tile and period, and therefore it was expected that they would better tackle the spatial and temporal variations of BA. The 10 × 10 tiles are the direct output from the pre-processing chain. It was decided to keep them as input to obtain the CDFs as this division offered a good balance between considering regional diversity and processing time. Use of land cover maps may have been helpful, but they would have also incorporated the inherent errors to any land cover product. Future versions would consider including this information in the algorithm, based on collaboration with the landcover_cci team.

The burned pixels to obtain the CDF of BA were obtained from the information provided by the MODIS HS. Since HS have an original resolution of 1000 × 1000 m, instead of assuming that all nine MERIS pixels covered by the HS pixel were active fires, we considered that the potential active fire (PAF) was more likely located at the minimum NIR value of the 3 × 3 window covered by the HS. To avoid commission errors, we introduced an additional temporal change constraint, and accepted as PAF only pixels that showed a NIR reflectance decrease in time t from the previous period (t − 1). The CDF of the unburned category was generated from the values of those pixels that did not have any HS in a 64 × 64 pixel matrix and that were not detected by the BA algorithm in the previous months.

The NIR threshold value of the burned category (TB) was defined by selecting the immediately lower decile of the burned pixels' CDF that intersected the first decile of the unburned pixels' CDF. This criterion implies in fact that we accepted to have as much as 10% commission error. The omission error would be estimated by the selected decile of the burned CDF. This omission was expected to be higher as the burned and unburned CDFs were closer, but it should be reduced in phase 2 (contextual analysis) of the algorithm.

Fig. 4 shows two examples of the CDFs to illustrate the computation of TB. In Fig. 4a) the CDFs of the burned and unburned classes are closer (implying poorer separation between both categories), while in Fig. 4b) the CDFs have better discriminability. In both cases, the criterion to select the TB was the same, but the actual TB value changed following the CDFs. In the former case, the TB was 0.108, corresponding to the NIR value of the fourth decile of the burned CDF, which was the lower close to the first decile of the unburned CDF. In the latter case, the TB value was 0.115, corresponding to the eight decile of the burned CDF. Therefore, the probability of omission would be lower than in the first case. This illustrates that the more separated the CDFs between burned and unburned categories were, the less chances of confusion. On the opposite, the closer the CDFs the more pixel values were shared by the burned and unburned distributions, and therefore more omission errors should be expected. For this reason, the decile used to define the TB was taken into account for phase 2 of the algorithm.

Once the TB was defined, pixels were considered BA seeds and therefore used for the contextual phase of the algorithm when three criteria were met:

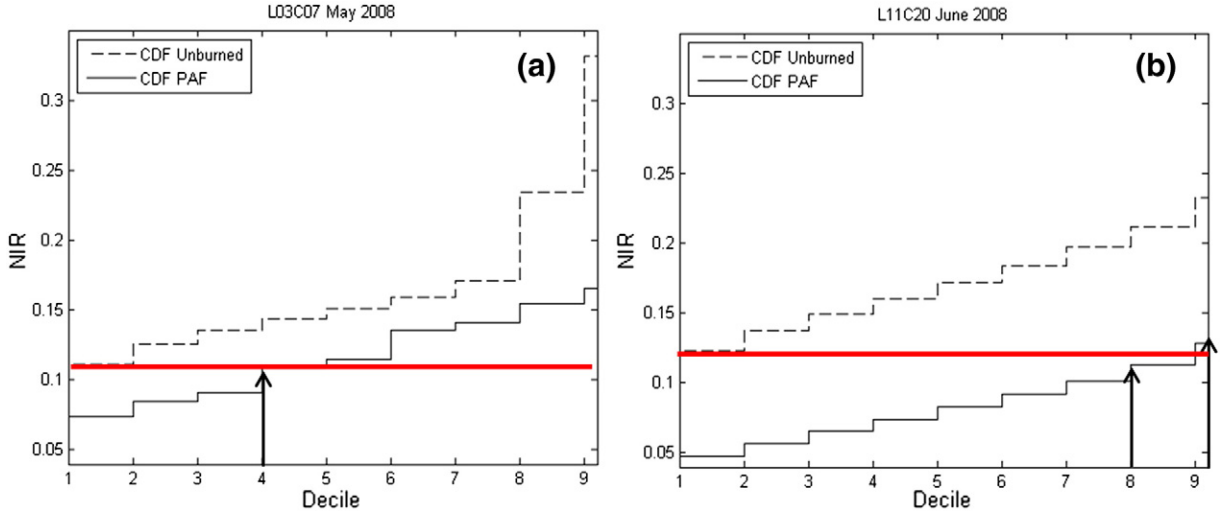

Fig. 4. Threshold based on decile 10 of the unburned CDF for cases with worse (a) and better (b) discrimination between classes, correspondent to May 2008 in tile L03C07 (Canada) and June 2008 in L11C20 (South Africa) respectively. In a) TB for seed and growing phases remains the same (single arrow). In b) TB for the seed phase corresponds to decile 8 (left arrow) and TB for the growing phase corresponds to decile 9 (right arrow).

a) The NIR value was lower than the computed TB of that tile and period.
b) At least one PAF should be found in a neighbour 9 × 9 matrix;
c) The NIR value for month t should be lower than the NIR value of month t − 1.

Fig. 5 includes a diagram that illustrates the main steps of seed and growing phases.

2.5. Region growing phase

Contextual algorithms have been previously used for BA mapping (Bastarrika et al., 2011b; Pu et al., 2007). The goal of these algorithms is to reduce omission errors that may result from the seed phase, while avoiding the increase of commission errors. One of the critical issues to obtain a good performance of these algorithms for BA mapping relies on obtaining a sound method to stop the region growing process (Zhang et al., 2005). Otherwise the iterative process may create severe overestimation.

For the MERIS BA algorithm only pixels surrounding the BA seeds were analysed for contextual analysis. This second phase of the BA algorithm included three growing conditions, which accounted for a proper balance between reducing omission errors (by extending the incomplete burned patches around seed pixels), while avoiding commission errors. Pixels around each seed were analysed recursively until they did not meet the growing conditions, which implied the end of the process (Fig. 5). If the criteria were met, the pixel was considered as a new seed and also its surrounding pixels were analysed.

The first condition implied that NIR values should be below TB, but the TB was less strict than in phase 1 if the CDFs of burned and unburned pixels were well separated. The criterion to increase or not the TB of the seed phase was based on which decile was used to establish the TB. When this value came from decile seventh or higher, the new TB was increased to the ninth decile of the burned CDF (Fig. 4b). Otherwise it was kept to the TB of the seed phase (Fig. 4a).

The second condition aimed to assure that the decrease in the NIR values (DNIR) between t and t − 1 for each candidate BA pixel was higher than the decrease observed for unburned areas. With this criterion, we tried to avoid neighbour areas to the seeds that might have fire-unrelated changes.

Finally, the third condition was based on detecting the vegetation loss as a result of fire, based on the differences in GEMI values between the target monthly composite and the annual GEMI composites. This criterion was defined as 0.9 times the difference found in the GEMI value between the target pixel and those labelled as burned (either original or new seeds).

A final test was applied to avoid large commission errors in a few areas with dark covers, where the region growing process did not perform properly (specific regions of Australia, China and India, for instance). In this case, we filtered out large polygons when the number of burned pixels largely exceeded the number of hotspots. We established an empirical value of 30 times (MERIS BA pixels/HS), based on previous findings from Hantson, Padilla, Corti, and Chuvieco (2013), who compared the distribution of HS and Landsat-derived burned patches in the same study sites used to develop this algorithm (Fig. 1).

2.6. Product assessment

Two assessments were performed with the MERIS BA results. The first one was based on a set of global validation sites, and the second one was an intercomparison with existing BA products. The methodology for the two approaches is introduced hereafter.

A complete global and temporal validation strategy has been developed within the Fire-CCI project (http://www.esa-fire-cci.org/webfm_send/779 last accessed November 26, 2014). The validation of the different BA products was performed using a statistically selected global sample of reference BA sites. The year 2008 was selected as the reference for validation following a CCI programmatic decision. Stratified random sampling was used to select 105 non-overlapping Thiessen scene areas (TSA), considering both ecosystem variation and historical fire occurrence (Padilla et al., 2014). Reference fire perimeters were generated by a semi-automatic BA algorithm developed by Bastarrika et al. (2011b, 2014) applied to two multi-temporal Landsat TM/ETM+ images for each sampled TSA. The reference files followed the standard protocol defined by the CEOS Cal-Val (http://lpvs.gsfc.nasa.gov/fire_home.html, last accessed November 26, 2014). Whenever the input images were ETM+, only the central strip of the images was processed, to avoid the impacts of the SLC-off gaps.

The validation metrics were derived from fuzzy error matrices to account for the different pixel size of TM/ETM and MERIS sensors. Six

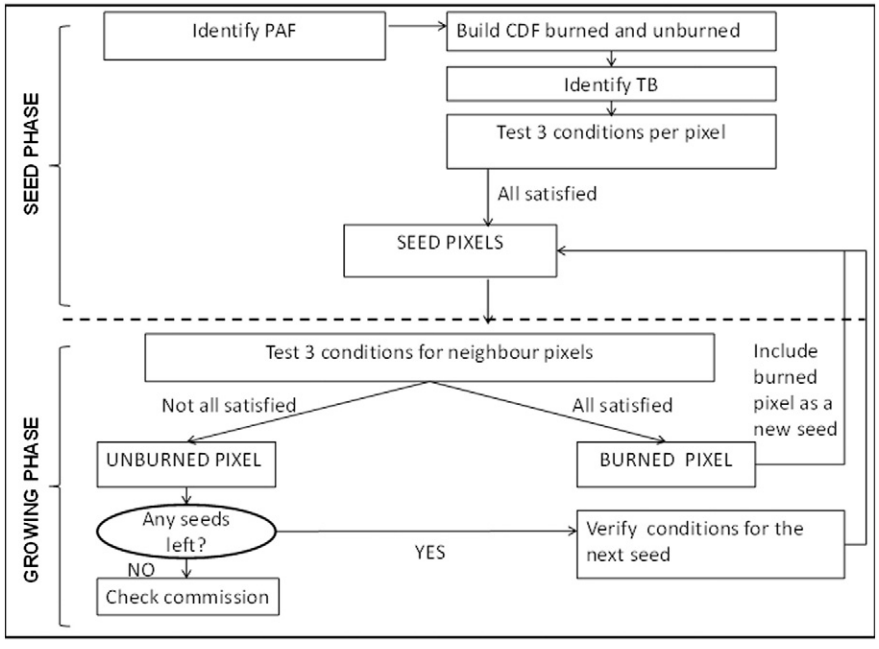

Fig. 5. Main steps of the algorithm: seed and growing phases.

accuracy measures were computed (overall accuracy, omission error, commission error, Dice coefficient, bias and relative bias) to satisfy criteria specified by end-users of burned area products. More details on the validation strategy can be found in Padilla et al. (2014) and Padilla et al. (2015).

The second assessment was based on intercomparison of spatial and temporal trends of our results with existing global BA products available for the same time series (2006–2008): GEOLAND-2, MCD45A1, and GFED v4. GEOLAND-2 was selected as representative of BA products based on European sensors, since the precursors (L3JRC and GlobCarbon) were not available for 2008, the key year for global validation. The two MODIS-based BA products (MCD45 and GFED v4) are currently the most broadly used in modelling studies (Mouillot et al., 2014).

2.7. Uncertainty

Uncertainty characterisation of the fire_cci products was based on a sample of study sites from 2006 to 2008 not used in the validation. A total of 23 pairs of Landsat TM/ETM + images were processed to generate these reference fire perimeters. For the MERIS pixel product (300 m), uncertainty was estimated in probabilistic terms (% confidence), based on regression analysis using as inputs the confidence level of the classification, the number of neighbour burned pixels, and the land cover. For the grid product, similar models were used, and the output was expressed as a standard error of the total burned area for each grid cell, following approaches of existing products (Giglio et al., 2010). Further details of the procedure can be found in the fire_cci project documentation (https://www.esa-fire-cci.org/webfm_send/791 last accessed November 26, 2014)

3. Results

3.1. Spatial and temporal trends

Three years of MERIS data (2006 to 2008) were processed with our algorithm. Total BA obtained with the MERIS algorithm ranges from 3.6 to 3.8 million km^2. In terms of spatial variability, Fig. 6 shows the gridded burned area obtained for 2008. The most extensive burnings occurred in the Tropical regions, particularly in the African continent, followed by the Northern regions of Australia, Central Brazil, Venezuelan and Colombian Llanos, and SE Asia. A second belt of burned regions is noticeable in the temperate grasslands and croplands of central Asia, and SE USA. The boreal forests of Russia and Canada have also a substantial role in global biomass burnings. Similar trends were obtained for 2006 and 2007.

The basic information used to compute BA was the date of detection, which showed seasonal trends of fire activity, with predominant January–March fires in the Northern Tropical belt, July–September in the Southern Tropical fringe, Northern Boreal and Temperate Regions of America and Eurasia. Fig. 7 includes the Julian dates of burn in Africa for 2008. The seasonal trends can be clearly identified for this case, with the fire peaks associated to the central months of the dry season.

Fig. 8 shows the estimation of uncertainty values for the same area, with a spatial variation associated mainly to the omission error, related to the availability of input images, with lower values for cloudy regions.

3.2. Validation

Table 3 shows the results of the validation metrics computed from the 105 global validation sites. They were divided in two subsamples, based on the proportion of burned area. The vast majority (100) had less than 10% of burned area, while only a few had more than that threshold. Overall accuracy was high in both cases (>87%), but BA accuracy was lower. Omission and commission errors were higher for those areas with very low burned area proportion than for those with more fire occurrence. The Dice coefficient (DC), which combines the omission and commission errors, was also higher for the sites with more BA proportion (0.48). Error balance (over and underestimation) was close to 0 for areas with larger BA, but showed underestimation for the overall sample and those areas with minor BA. In relative terms (relB) the overall sample showed BA underestimation by 34%.

Comparison with existing BA products showed that MERIS BA results have similar overall accuracy than the two MODIS BA products (MCD45 and MCD64) (OA > 0.99), but it showed significantly higher commission and omission errors than MCD64 (CE = 0.42; OE = 0.68), and higher commission error than MCD45 (CE = 0.46; OE = 0.72) (Padilla et al., 2015). The errors found with the MERIS product were significantly lower than the ones from existing European BA products. In terms of error balance, the estimations showed different trends for areas with very small BA and for those with higher BA proportion, but an overall trend towards underestimation was observed. The relative balance of errors showed better results than MCD64 and MCD45 with a 34% of underestimation for MERIS, versus 44% for MCD64 and 48% for MCD45 (Padilla et al., 2015).

3.3. Intercomparison with existing products

Table 4 includes total BA estimations from the MERIS BA product and from the MODIS-based (MCD45 and MCD64) products for the three years when global outputs were available. GFED v4 is derived from the MCD64A1 product aggregated to 0.25° spatial resolution for the period 2000–present. Prior to 2000, GFED BA estimates are obtained by calibrating active fire data from the Tropical Rainfall Measuring Mission (TRMM), Visible and Infrared Scanner (VIRS) and Along-Track Scanning Radiometer (ATSR) with the MCD64A1. MERIS BA estimates are 3 to 9% higher than GFED v4 and 7–9% higher than MCD45.

In terms of spatial distribution of BA Fig. 9 illustrates the GFED v4, MCD45, GEOLAND2 and MERIS_CCI BA products in 2008 separated by ecoregion (following the geographical ecoregions defined by Giglio, van der Werf, Randerson, Collatz, & Kasibhatla, 2006). The vast majority of BA occurred in the two African hemispheres (NHAF, SHAF, summing both 70% of total), followed by far by Australia, Central Asia, South America and Boreal Asia. For nine regions (CEAM, EQAS, EURO, MIDE, NHAF, SEAS, SHAF, SHSA, and TENA) MERIS estimates were higher or in the same order as the GFED v4 and MCD45 ones. GEOLAND2 reported higher values in boreal and temperate regions (BOAS, BONA, CEAS and TENA) and significantly lower in Tropical areas (NHAF and SHAF). Overall, a high level of agreement was found between MERIS, GFED v4 and MCD45 ($r^2 > 0.99$).

When looking at seasonal trends, a high level of agreement was also found between MERIS and existing BA products. Fig. 10 includes monthly estimations by MERIS and GFED v4 of global BA from 2006 to 2008. According to the figure, the trend between products was consistent in terms of magnitude through the temporal series. GFED v4 underestimates when compared to MERIS, except for October, November 2006 and July and August 2007 and 2008.

4. Discussion

This paper presents the first global algorithm to detect burned areas from MERIS ENVISAT imagery. Even though the sensor's temporal and spectral characteristics are not optimal for BA detection, we have shown that MERIS images complemented with HS information can provide reliable estimations of BA. Certainly, MERIS is no longer available (as ENVISAT mission ended in 2012). However, a long time series (2003 to 2012) could be computed from this algorithm, thus providing a complementary view on the existing knowledge of BA trends. In addition, the future ESA Sentinel-3 satellite (to be launched in 2015) will include a similar sensor (OLCI), which could benefit from our algorithm to build a semi-operational BA product. As this satellite will also incorporate a thermal sensor (the SLSTR), with active fire detection capabilities, the

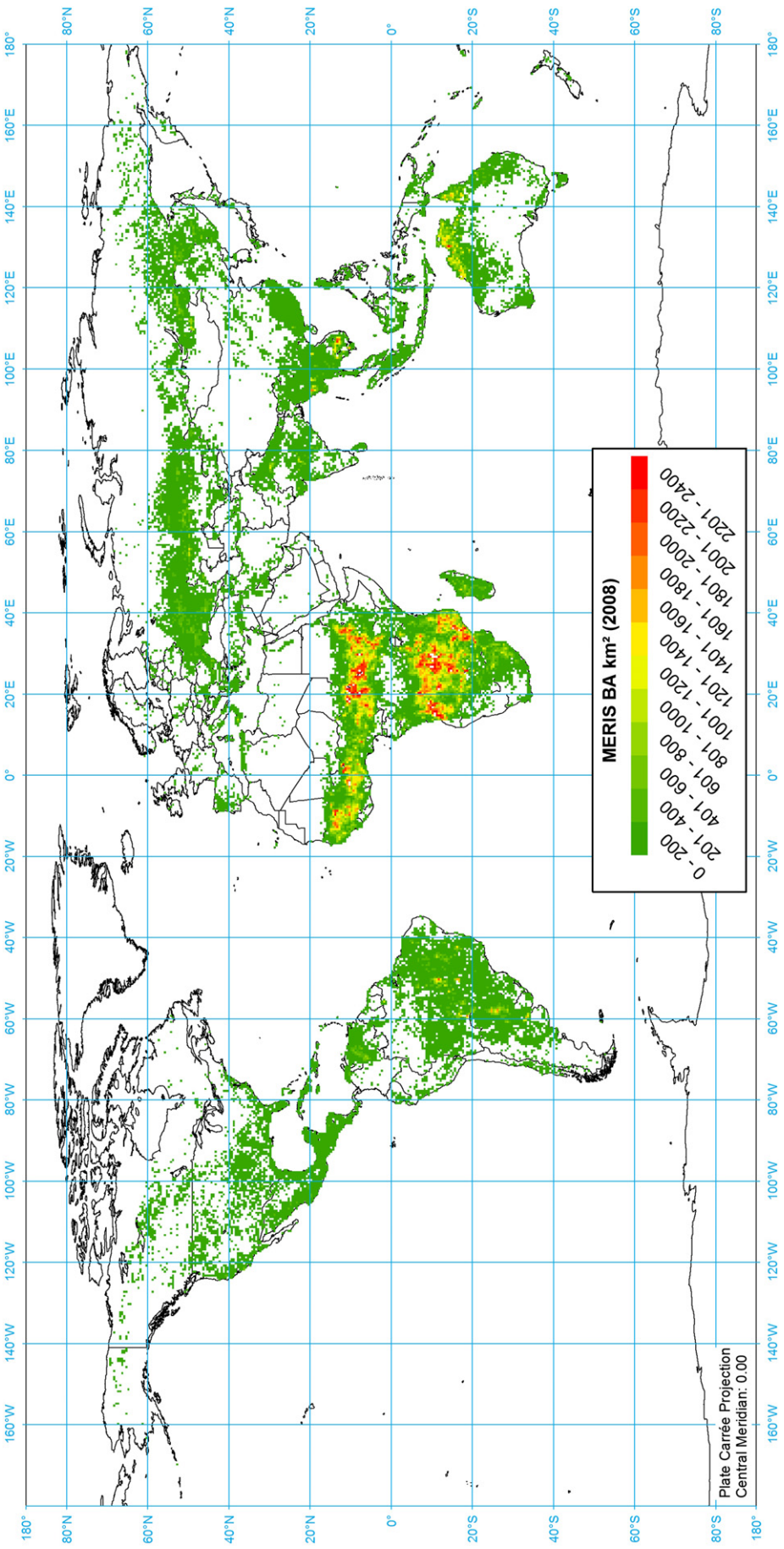

Fig. 6. MERIS global BA for 2008.

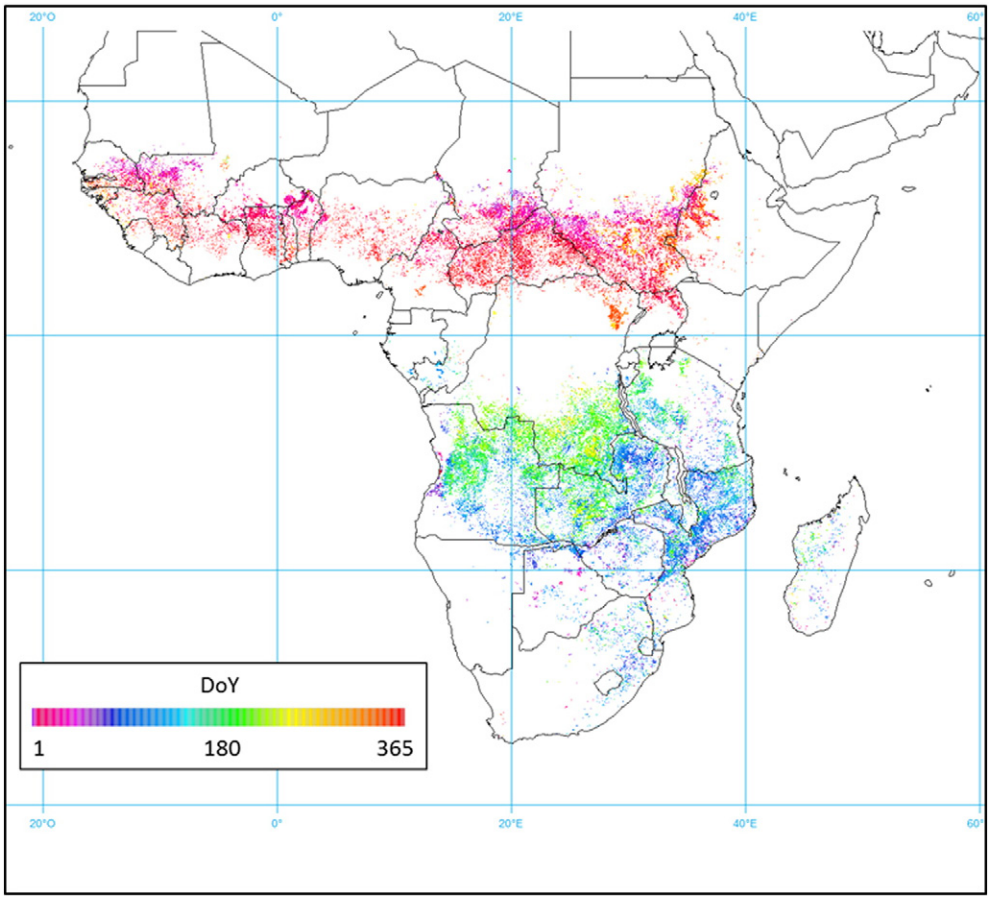

Fig. 7. MERIS burn detection dates for Africa in 2008.

methods presented in this paper could be implemented without the need of using data from other satellites. On the other hand, our hybrid approach can also be useful for other sensors that are constrained to the red-near infrared space, as it is the case of the higher spatial resolution (250 m) bands of MODIS.

Since our algorithm relies on MODIS HS and MERIS reflectance information, the results cannot be considered fully independent from MODIS products, particularly from MCD64, which uses a hybrid approach as well. However, the structure of the algorithm is quite different from Giglio et al. (2009), and it is built on the particular spectral space detected by the MERIS sensor. Spatial variations between our results and GFED v4 for instance, show that HS input does not fully determine the output results.

Our hybrid approach takes advantage from both the more sensitive thermal characterisation of active fires and the more permanent reflectance changes of burned patches. HS information helped establishing regional thresholds for BA discrimination, while mitigating potential commission errors. However, the use of HS also implies a certain contribution to overall BA error (not yet fully assessed in our results). HSs have proven very reliable to detect active fires, with very low commission error, but they are not frequent or sensitive enough to detect all active fires, and therefore omission errors are higher (Csiszar, Denis, Giglio, Justice, & Hewson, 2005; Giglio, Csiszar, & Justice, 2006; Hantson et al., 2013). Alternative criteria based on change detection techniques to complement HS information were considered in our project, particularly in those regions where omissions are more relevant, but could not finally be implemented due to the low temporal frequency of MERIS acquisitions (Fig. 2). This omission error inherent to HS is also included in other BA products based on HS (such as the GFED-MCD64). An improved seed procedure with very clear fire-related reflectance changes may be included in future versions, ensuring also more independency from the thermal information. However, additional research is needed to build more robust time series from MERIS reflectance data. This could be achieved also from its successor, the OLCI on board Sentinel 3, since temporal coverage will improve (revisit time will be 2.2 days with one satellite and 1.1 day when both satellites are launched).

The two assessment exercises presented in this paper confirmed that MERIS algorithm provided acceptable results. When estimating total BA in the statistically designed validation sample, MERIS provided lower but comparable accuracy metric values to the MODIS-based BA products (MCD45 and MCD64). Overall accuracy showed very high values (OA > 0.95), but the product showed higher commission errors (CE = 0.64) than MCD64 and MCD45 and similar omission errors (OE = 0.76) to the MCD45. The relative balance of errors showed better results than MCD64 and MCD45 with a 34% of underestimation. Errors were lower for the areas with higher proportion of burned area (OE = 0.51 and CE = 0.52; Table 3). MERIS errors were significantly lower than the ones obtained with other European BA products (Padilla et al., 2015).

These estimations of errors may be considered pessimistic, as some of these errors are in fact caused by the low temporal frequency of the MERIS sensor. We computed the temporal reporting accuracy of our results by obtaining the difference between MERIS BA detection dates and HS dates. We observed that 50% of the MERIS detections occurred with a difference of 4 to 22 days from the HS in four test sites (>250,000 km^2) located in Tropical (Australia), Temperate (California and the Iberian Peninsula) and Boreal (Canada) ecosystems, reaching up to 9–30 days when the threshold was increased to 75%. The temporal accuracy was therefore lower than the values obtained globally by Boschetti et al. (2010) for the MCD45 product (50% within one day and 75% within four days). The low MERIS reporting accuracy increases the likelihood of omission and commission errors, particularly when the two Landsat

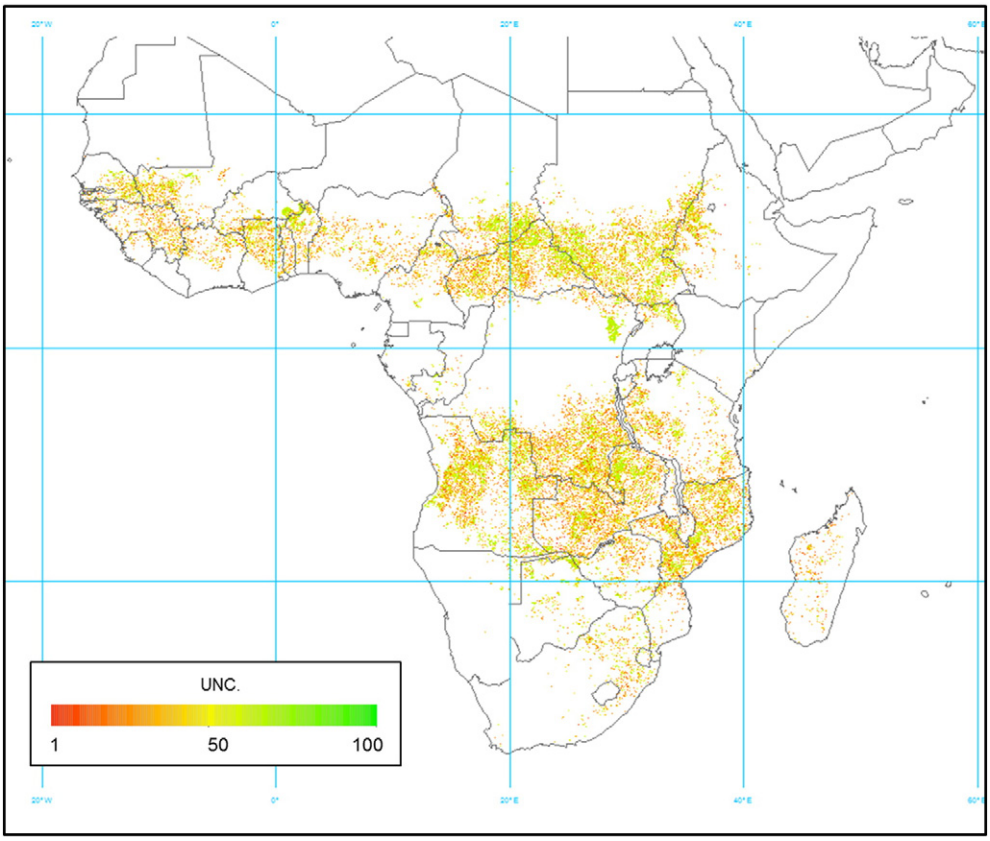

Fig. 8. Uncertainty relative to MERIS BA estimates for Africa in 2008.

images used to obtain the reference perimeters were close in time (as it was the case of Tropical ecosystems where most validation pairs of images were separated by 32 days or less). In fact, when comparing our results for 2008 with existing fire perimeters in the four test sites where temporal accuracy was tested (Australia, California, Iberian Peninsula and Canada), we found that both commission and omission errors decreased to 0.47 and 0.15 respectively. This reduction of detection errors compared to the Landsat validation sample should be related to the longer period included in the test sites (which covers the full year), when dating errors are expected to affect marginally the accuracy estimations.

Our results showed similar estimations to existing BA products, both in terms of total BA values, and geographical distribution, with better estimations (according to validation results) than existing European BA products, particularly in Tropical regions. Further comparison of the MERIS results with GFED v4, one of the most widely used by climate modellers, showed similar temporal trends for the 3 years processed. Global estimations were 3 to 9% higher than GFED v4 for the three years computed, while geographical and monthly trends showed high correlation values.

However, our MERIS results still show some detection problems, particularly in temperate regions, where fires are unusual and commission errors were found by misclassification with agricultural areas. In Tropical regions, omissions were higher, which may be caused by the errors associated to the HS detections, becoming more relevant in areas with small fires (Hantson et al., 2013). In addition, the conditions for contextual analysis should be reviewed for future versions of the algorithm, particularly in relation to fragmentation of fires and in cloudy areas that caused temporal gaps in the MERIS time series.

5. Conclusions

A hybrid algorithm to estimate burned areas on a global scale from MERIS reflectance and MODIS HS time series was developed within the framework of the Climate Change Initiative of the European Space Agency. This algorithm makes use of thermal, NIR and visible information to detect burned pixels. It is based on a two-step process: seed and growing phases. Results were obtained for three years of data, estimating a total BA from 3.6 to 3.8 million km^2. Patterns of fire activity were also identified (African Tropical regions, Northern regions of Australia, Central Brazil, Central and South East Asia, Russia, Canada and South East USA) as well as seasonal trends. MERIS BA estimates showed similar although lower accuracy than existing MODIS BA products, based on a validation dataset produced from multitemporal Landsat images. Some of the observed errors were related

Table 3
Estimated accuracy metrics for MERIS BA.

OA	DC	Ce	Oe	B	relB	Burned area proportion
0.9581	0.312	0.597	0.745	−0.0137	−0.3657	<0.1
0.879	0.486	0.517	0.510	0.0018	0.0157	>0.1
0.996	0.290	0.640	0.760	−0.12	−0.34	All

Table 4
GFED v4, MCD45 and MERIS BA in km^2 for years 2006 to 2008.

	GFED v4	MCD45	MERIS_CCI
2006	3,417,863	3,374,125	3,652,355
2007	3,644,122	3,523,728	3,773,855
2008	3,307,377	3,308,200	3,624,146

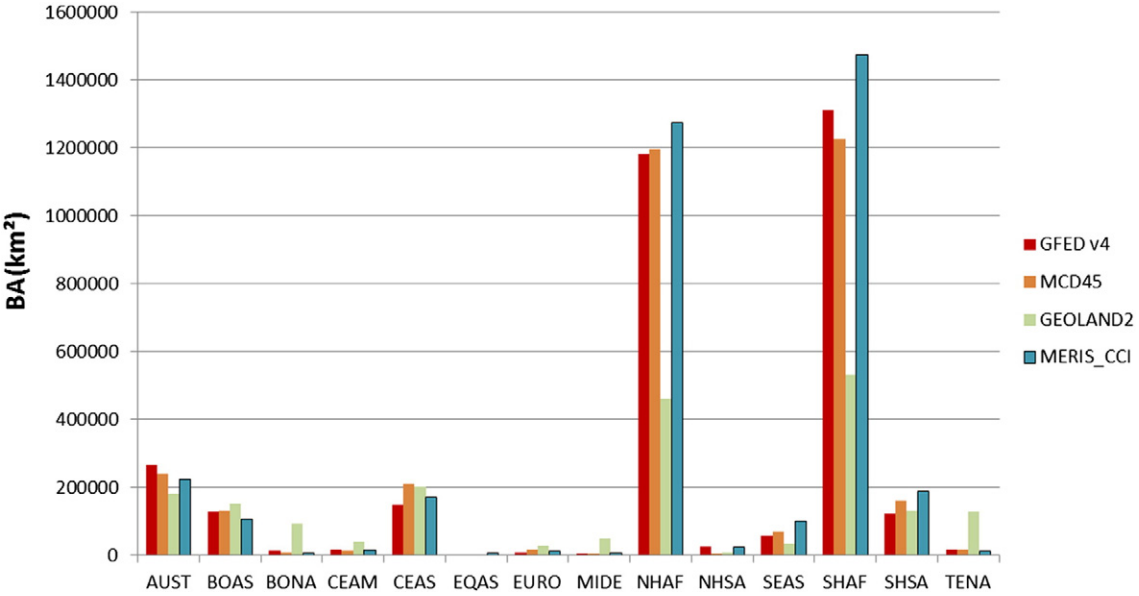

Fig. 9. BA 2008 estimations for MCD45, GFED v4, GEOLAND2 and MERIS_CCI for the 14 ecoregions defined in Giglio, van der Werf, Randerson, Collatz and Kasibhatla (2006) (BONA = Boreal North America, TENA = Temperate North America, CEAM = Central America, NHSA = Northern Hemisphere South America, SHSA Southern Hemisphere South America, EURO = Europe, MIDE = Middle East Africa, NHAF = Northern Hemisphere Africa, SHAF = Southern Hemisphere Africa, BOAS = Boreal Asia, CEAS = Central Asia, SEAS = Southeast Asia, EQAS = Equatorial Asia, AUST = Australia).

to temporal reporting problems associated to the MERIS coverage frequency.

This algorithm will be the basis for computing a full BA time series for the second phase of the fire_cci project (2003 to 2012), while preparing the upcoming generations of the European Space Agency burned area products, particularly those based on Sentinel-3 OLCI-SLSTR sensors. The availability of alternative BA time series would complement existing BA products, providing more robust estimations and improvements in the uncertainty characterisation of BA inputs for climate models (Mouillot et al., 2014). On the other hand, different BA products can provide diverse regional accuracies and therefore, merging outputs from global synthesis may greatly improve how BA trends are currently characterised.

Acknowledgements

This work was developed within the Fire-CCI project, in the framework of the European Space Agency Climate Change Initiative programme. Early developments of the MERIS algorithm were produced by Teresa Calado, Patricia Oliva and Federico González, all part of the fire_cci project consortium. The validation dataset was generated by Marc Padilla, Stijn Hantson, Dante Corti, and Ruben Ramo. Validation metrics were developed by Marc Padilla. Intercomparison analysis with existing BA products was partially computed by Ruben Ramo.

The final MERIS BA product can be freely downloaded from the web page of the fire_cci project: http://www.esa-fire-cci.org/ (last accessed November 26, 2014).

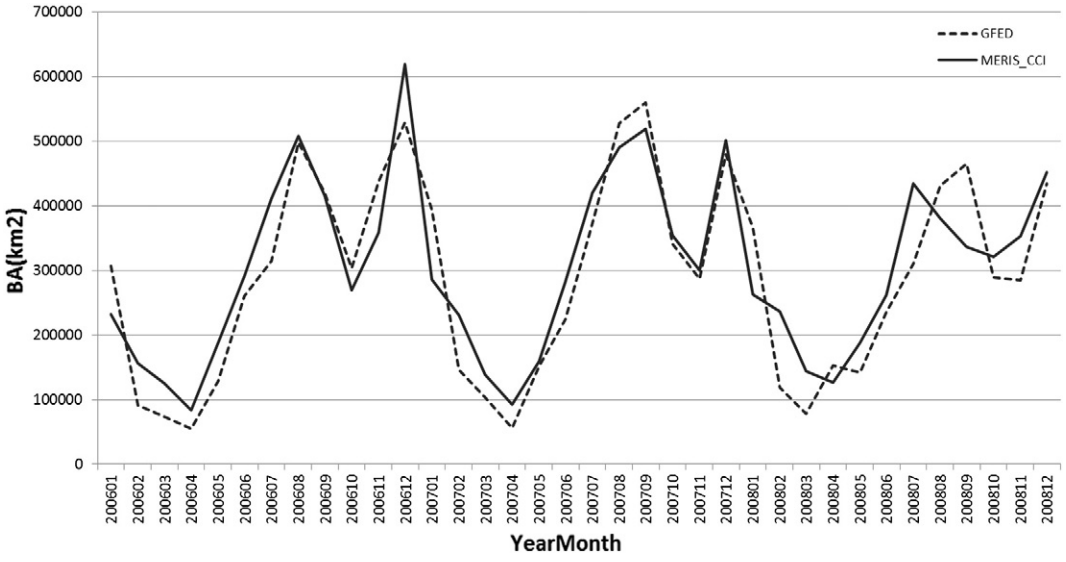

Fig. 10. Monthly global BA in 2006 to 2008 for MERIS_CCI and GFED v4.

References

Andreae, M. O., & Merlet, P. (2001). Emission of trace gases and aerosols from biomass burning. *Global Biogeochemical Cycles*, *15*, 955–966.

Barbosa, P. M., Grégoire, J. M., & Pereira, J. M. C. (1999). An algorithm for extracting burned areas from time series of AVHRR GAC data applied at a continental scale. *Remote Sensing of Environment*, *69*, 253–263.

Bastarrika, A., Alvarado, M., Artano, K., Martinez, M., Mesanza, A., Torre, L., et al. (2014). BAMS: A tool for supervised burned area mapping using Landsat data. *Remote Sensing*, *6*, 12360–12380.

Bastarrika, A., Chuvieco, E., & Martin, M. P. (2011a). Automatic burned land mapping from MODIS time series images: Assessment in Mediterranean ecosystems. *IEEE Transactions on Geoscience and Remote Sensing*, *49*, 3401–3413.

Bastarrika, A., Chuvieco, E., & Martin, M. P. (2011b). Mapping burned areas from Landsat TM/ETM+ data with a two-phase algorithm: Balancing omission and commission errors. *Remote Sensing of Environment*, *115*, 1003–1012.

Boschetti, L., Eva, H. D., Brivio, P. A., & Gregoire, J. M. (2004). Lessons to be learned from the comparison of three satellite-derived biomass burning products. *Geophysical Research Letters*, *31*, L21501 (21510.21029/22004GL021229).

Boschetti, L., Roy, D. P., Justice, C. O., & Giglio, L. (2010). Global assessment of the temporal reporting accuracy and precision of the MODIS burned area product. *International Journal of Wildland Fire*, *19*, 705–709.

Bourg, L. (2011). *The AMORGOS MERIS CFI (Accurate MERIS Ortho-Rectified Geo-location Operational Software) processing.* Validation report (PO-RP-ACR-GS-0014) ACRI-ST.

Bowman, D. M. J. S., Balch, J. K., Artaxo, P., Bond, W. J., Carlson, J. M., Cochrane, M. A., et al. (2009). Fire in the Earth system. *Science*, *324*, 481–484.

Brassel, K. E., & Reif, D. (1979). A procedure to generate Thiessen polygons. *Geographical Analysis*, *11*, 289–303.

Carmona-Moreno, C., Belward, A., Malingreau, J. P., Hartley, A., Garcia-Alegre, M., Antonovskiy, M., et al. (2005). Characterizing interannual variations in global fire calendar using data from Earth observing satellites. *Global Change Biology*, *11*, 1537–1555.

Chang, D., & Song, Y. (2009). Comparison of L3JRC and MODIS global burned area products from 2000 to 2007. *Journal of Geophysical Research*, *114*. http://dx.doi.org/10.1029/2008JD11361.

Chuvieco, E., De Santis, A., Riaño, D., & Halligan, K. (2007). Simulation approaches for burn severity estimation using remotely sensed images. *Journal of Fire Ecology*, *3*, 129–150.

Chuvieco, E., Englefield, P., Trishchenko, A. P., & Luo, Y. (2008a). Generation of long time series of burn area maps of the boreal forest from NOAA–AVHRR composite data. *Remote Sensing of Environment*, *112*, 2381–2396.

Chuvieco, E., Martín, M. P., & Palacios, A. (2002). Assessment of different spectral indices in the red-near-infrared spectral domain for burned land discrimination. *International Journal of Remote Sensing*, *23*, 5103–5110.

Chuvieco, E., Opazo, S., Sione, W., Del Valle, H., Anaya, J., Di Bella, C., et al. (2008b). Global burned land estimation in Latin America using MODIS composite data. *Ecological Applications*, *18*, 64–79.

Chuvieco, E., Ventura, G., Martín, M. P., & Gomez, I. (2005). Assessment of multitemporal compositing techniques of MODIS and AVHRR images for burned land mapping. *Remote Sensing of Environment*, *94*, 450–462.

Csiszar, I., Denis, L., Giglio, L., Justice, C. O., & Hewson, J. (2005). Global fire activity from two years of MODIS data. *International Journal of Wildland Fire*, *14*, 117–130.

Daniau, A. L., Bartlein, P. J., Harrison, S. P., Prentice, I. C., Brewer, S., Friedlingstein, P., et al. (2012). Predictability of biomass burning in response to climate changes. *Global Biogeochemical Cycles*, *26*.

Ershov, D. V., & Novik, V. P. (2001). Mapping burned areas in Russia with spot4 vegetation (S1 product) imagery. *Final report, Contract 18176-2001-07-F1EI ISP RU, Eur. Comm. Joint Res. Cent., Brussels*.

Eva, H., & Lambin, E. F. (1998). Burnt area mapping in Central Africa using ATSR data. *International Journal of Remote Sensing*, *19*, 3473–3497.

Fraser, R. H., Li, Z., & Cihlar, J. (2000). Hotspot and NDVI differencing synergy (HANDS): A new technique for burned area mapping over boreal forest. *Remote Sensing of Environment*, *74*, 362–376.

Giglio, L., Csiszar, I., & Justice, C. O. (2006a). Global distribution and seasonality of active fires as observed with the Terra and Aqua Moderate Resolution Imaging Spectroradiometer (MODIS) sensors. *Journal of Geophysical Research-Biogeosciences*, *111*. http://dx.doi.org/10.1029/2005JG000142.

Giglio, L., van der Werf, G. R., Randerson, J. T., Collatz, G. J., & Kasibhatla, P. (2006b). Global estimation of burned area using MODIS active fire observations. *Atmospheric Chemistry and Physics*, *6*, 957–974.

Giglio, L., Loboda, T., Roy, D. P., Quayle, B., & Justice, C. O. (2009). An active-fire based burned area mapping algorithm for the MODIS sensor. *Remote Sensing of Environment*, *113*, 408–420.

Giglio, L., Randerson, J. T., van der Werf, G. R., Kasibhatla, P. S., Collatz, G. J., Morton, D. C., et al. (2010). Assessing variability and long-term trends in burned area by merging multiple satellite fire products. *Biogeosciences Discuss*, *7*, 1171–1186 (1110.5194/bg-1177-1171-2010).

González-Alonso, F., Salgado, V., Calle, V., Casanova, J. L., Sanz, J., de la Fuente, D., et al. (2009). Forest burn in China by means of MERIS and MODIS images. *Dragon 2 Symposium, June 2009, Barcelona*.

Gower, J. F. R., & Borstad, G. A. (2004). On the potential of MODIS and MERIS for imaging chlorophyll fluorescence from space. *International Journal of Remote Sensing*, *25*, 1459–1464.

Grégoire, J. M., Tansey, K., & Silva, J. M. N. (2003). The GBA2000 initiative: Developing a global burned area database from SPOT-VEGETATION imagery. *International Journal of Remote Sensing*, *24*, 1369–1376.

Hantson, S., Padilla, M., Corti, D., & Chuvieco, E. (2013). Strengths and weaknesses of MODIS hotspots to characterize global fire occurrence. *Remote Sensing of Environment*, *131*, 152–159.

Hollmann, R., Merchant, C. J., Saunders, R. W., Downy, C., Buchwitz, M., Cazenave, A., et al. (2013). The ESA climate change initiative: Satellite data records for essential climate variables. *Bulletin of the American Meteorological Society*. http://dx.doi.org/10.1175/BAMS-D-11-00254.1.

Huang, S., & Siegert, F. (2004). ENVISAT multisensor data for fire monitoring and impact assessment. *International Journal of Remote Sensing*, *25*, 4411–4416.

Kachmar, M., & Sanchez-Azofeifa, G. A. (2006). Detection of post-fire residuals using high- and medium-resolution satellite imagery. *Forestry Chronicle*, *82*, 177–186.

Kasischke, E. S., French, N. H. F., Harrell, P., Christensen, N. L., Ustin, S. L., & Barry, D. (1993). Monitoring of wildfires in boreal forests using large area AVHRR NDVI composite image data. *Remote Sensing of Environment*, *45*, 61–71.

Kloster, S., Mahowald, N., Randerson, J., & Lawrence, P. (2012). The impacts of climate, land use, and demography on fires during the 21st century simulated by CLM-CN. *Biogeosciences*, *9*, 509–525.

Koutsias, N., & Karteris, M. (2000). Burned area mapping using logistic regression modeling of a single post-fire Landsat-5 Thematic Mapper image. *International Journal of Remote Sensing*, *21*, 673–687.

Krawchuk, M. A., Moritz, M. A., Parisien, M. -A., Van Dorn, J., & Hayhoe, K. (2009). Global pyrogeography: The current and future distribution of wildfire. *PLoS One*, *4*, e5102.

Martín, M.P., Gómez, I., & Chuvieco, E. (2005). Performance of a burned-area index (BAIM) for mapping Mediterranean burned scars from MODIS data. In J. Riva, F. Pérez-Cabello, & E. Chuvieco (Eds.), *Proceedings of the 5th International Workshop on Remote Sensing and GIS applications to Forest Fire Management: Fire Effects Assessment* (pp. 193–198). Paris: Universidad de Zaragoza, GOFC-GOLD, EARSeL.

Mouillot, F., & Field, C. B. (2005). Fire history and the global carbon budget: a 1 degrees × 1 degrees fire history reconstruction for the 20th century. *Global Change Biology*, *11*, 398–420.

Mouillot, F., Schultz, M. G., Yue, C., Cadule, P., Tansey, K., Ciais, P., et al. (2014). Ten years of global burned area products from spaceborne remote sensing — A review: Analysis of user needs and recommendations for future developments. *International Journal of Applied Earth Observation and Geoinformation*, *26*, 64–79.

Oliva, P., Martin, P., & Chuvieco, E. (2011). Burned area mapping with MERIS post-fire image. *International Journal of Remote Sensing*, *32*, 4175–4201.

Padilla, M., Stehman, S. V., & Chuvieco, E. (2014). Validation of the 2008 MODIS-MCD45 global burned area product using stratified random sampling. *Remote Sensing of Environment*, *144*, 187–196.

Padilla, M., Stehman, S. V., Ramo, R., Corti, D., Hantson, S., Oliva, P., et al. (2015). Comparing the accuracies of remote sensing global burned area products using stratified random sampling and estimation. *Remote Sensing of Environment*, *160*, 114–121.

Pechony, O., & Shindell, D. (2010). Driving forces of global wildfires over the past millennium and the forthcoming century. *Proceedings of the National Academy of Sciences*, *107*, 19167–19170.

Pereira, J. M. C. (1999). A comparative evaluation of NOAA/AVHRR vegetation indexes for burned surface detection and mapping. *IEEE Transactions on Geoscience and Remote Sensing*, *37*, 217–226.

Piccolini, I., & Arino, O. (2000). Towards a global burned surface world atlas. *Earth Observation Quarterly*, *65*, 14–18.

Pinty, B., & Verstraete, M.M. (1992). GEMI: A non-linear index to monitor global vegetation from satellites. *Vegetatio*, *101*, 15–20.

Plummer, S., Arino, O., Ranera, F., Tansey, K., Chen, J., Dedieu, G., et al. (2007). An update on the GlobCarbon initiative: Multi-sensor estimation of global biophysical products for global terrestrial carbon studies. *Envisat Symposium. Montreux, Switzerland: ESA SP-636*.

Pu, R., & Gong, P. (2004). Determination of burnt scars using logistic regression and neural network techniques from a single post-fire Landsat-7 ETM+ image. *Photogrammetric Engineering and Remote Sensing*, *70*, 841–850.

Pu, R. L., Li, Z. Q., Gong, P., Csiszar, I., Fraser, R., Hao, W. -M., et al. (2007). Development and analysis of a 12-year daily 1-km forest fire North America from NOAA/AVHRR data. *Remote Sensing of Environment*, *108*, 198–208.

Riaño, D., Ruiz, J. A. M., Isidoro, D., Ustin, S. L., & Riaño, D. (2007). Global spatial patterns and temporal trends of burned area between 1981 and 2000 using NOAA-NASA Pathfinder. *Global Change Biology*, *13*, 40–50. http://dx.doi.org/10.1111/j.1365-2486.2006.01268.

Roldan-Zamarron, A., Merino-De-Miguel, S., Gonzalez-Alonso, F., Garcia-Gigorro, S., & Cuevas, J. M. (2006). Minas de Riotinto (south Spain) forest fire: Burned area assessment and fire severity mapping using Landsat 5-TM, Envisat-MERIS, and Terra-MODIS postfire images. *Journal of Geophysical Research-Biogeosciences*, *111*.

Roy, D. P., & Boschetti, L. (2009). Southern Africa validation of the MODIS, L3JRC and GlobCarbon burned-area products. *IEEE Transactions on Geoscience and Remote Sensing*, *47*. http://dx.doi.org/10.1109/TGRS.2008.2009000.

Roy, D. P., Boschetti, L., & Justice, C. O. (2008). The collection 5 MODIS burned area product — Global evaluation by comparison with the MODIS active fire product. *Remote Sensing of Environment*, *112*, 3690–3707.

Roy, D. P., Giglio, L., Kendall, J. D., & Justice, C. O. (1999). Multi-temporal active-fire based burn scar detection algorithm. *International Journal of Remote Sensing*, *20*, 1031–1038.

Roy, D., Jin, Y., Lewis, P., & Justice, C. (2005). Prototyping a global algorithm for systematic fire-affected area mapping using MODIS time series data. *Remote Sensing of Environment*, *97*, 137–162.

Running, S. W. (2006). Is global warming causing more, larger wildfires? *Science*, *313*, 927–928.

Silva, J. M. N., Pereira, J. M. C., Cabral, A. I., Sa, A. C. L., Vasconcelos, M. J. P., Mota, B., et al. (2003). An estimate of the area burned in southern Africa during the 2000 dry season using SPOT-VEGETATION satellite data. *Journal of Geophysical Research-Atmospheres*, *108*.

Simon, M., Plummer, S., Fierens, F., Hoelzemann, J. J., & Arino, O. (2004). Burnt area detection at global scale using ATSR-2: The GLOBSCAR products and their qualification. *Journal of Geophysical Research-Atmospheres*, *109*, D14S02. http://dx.doi.org/10.1029/2002JD003622 (1-16).

Sousa, A. M. O., Pereira, J. M. C., & Silva, J. M. N. (2003). Evaluating the performance of multitemporal image compositing algorithms for burned area analysis. *International Journal of Remote Sensing*, *24*, 1219–1236.

Sukhinin, A. I., French, N. H. F., Kasischke, E. S., Hewson, J. H., Soja, A. J., Csiszar, I. A., et al. (2004). AVHRR-based mapping of fires in Russia: New products for fire management and carbon cycle studies. *Remote Sensing of Environment*, *93*, 546–564.

Tansey, K., Grégoire, J.M., Defourny, P., Leigh, R., Peckel, J. F., Bogaert, E. V., et al. (2008). A new, global, multi-annual (2000–2007) burnt area product at 1 km resolution. *Geophysical Research Letters*, *35*, L01401. http://dx.doi.org/10.1029/2007GL03156.

Tansey, K., Grégoire, J. M., Stroppiana, D., Sousa, A., Silva, J., Pereira, J. M., et al. (2004). Vegetation burning in the year 2000: Global burned area estimates from SPOT VEGETATION data. *Journal of Geophysical Research-Atmospheres*, *109*, D14S03. http://dx.doi.org/10.1029/2002JD003598 (2–22).

Thonicke, K., Spessa, A., Prentice, I. C., Harrison, S. P., Dong, L., & Carmona-Moreno, C. (2010). The influence of vegetation, fire spread and fire behaviour on biomass burning and trace gas emissions: Results from a process-based model. *Biogeosciences*, *7*, 1991–2011.

Trigg, S., & Flasse, S. (2001). An evaluation of different bi-spectral spaces for discriminating burned shrub-savannah. *International Journal of Remote Sensing*, *22*, 2641–2647.

van der Werf, G. R., Randerson, J. T., Giglio, L., Collatz, G., Mu, M., Kasibhatla, P. S., et al. (2010). Global fire emissions and the contribution of deforestation, savanna, forest, agricultural, and peat fires (1997–2009). *Atmospheric Chemistry and Physics*, *10*, 11707–11735.

Zhang, Q. F., Pavlic, G., Chen, W. J., Fraser, R., Leblanc, S., & Cihlar, J. (2005). A semi-automatic segmentation procedure for feature extraction in remotely sensed imagery. *Computers & Geosciences*, *31*, 289–296.